

Performance Analysis of Pair-wise Symbol Detection in Uplink NOMA-ISaC Systems

Haofeng Liu, *Graduate Student Member, IEEE*, Emad Alsusa, *Senior Member, IEEE*,
and Arafat Al-Dweik, *Senior Member, IEEE*

Abstract—This paper investigates the bit error rate (BER) and outage probability performance of integrated sensing and communication (ISaC) in uplink non-orthogonal multiple access (NOMA) based Internet of Things (IoT) systems. Specifically, we consider an ISaC system where the radar signal is designed to be orthogonal to the communication signal over two symbol periods so that its interference on the communication signal is completely eliminated when detecting the data in pairs of consecutive symbols. This is akin to multi-symbol rate NOMA systems except in this case as the radar bears no data, its waveform is manipulated to be orthogonal to the transmitted communication signal. To eliminate potential decision ambiguity during the pair-wise data detection, a constant phase-offset between adjacent communication symbols is applied at the transmitter. The performance of such a system is analyzed through deriving analytical expressions for the exact BER of zero-forcing (ZF) based receivers. In addition, close-form expressions for the upper BER bound and the outage probability for both ZF and the joint maximum likelihood (JML) receivers are presented. The results show that the derived expressions are perfectly matched with the simulation results. The obtained expressions provide an insight into the performance of this novel ISaC system including demonstrating the impact of various parameters and showing how the ZF receiver provides a useful trade-off between performance and complexity relative to the JML receiver.

Index Terms—Uplink non-orthogonal multiple access (NOMA), integrated sensing and communication (ISaC), bit error rate (BER), outage probability.

I. INTRODUCTION

THE advent of 6th generation (6G) communication systems brings a paradigm shift toward integrating communication with radar detection capabilities, which is crucial for applications such as the location of unmanned aerial vehicle (UAV) and automated industrial processes [1]. In addition, Internet of Things (IoT) devices play a key role in perfecting communication and radar detection technologies with their ubiquitous sensors and interconnections. By leveraging a dense network of IoT sensors, 6G systems can achieve unprecedented levels of environmental awareness and data collection. [2] However, the growing number of mobile devices presents a significant challenge in satisfying both the demands of communication and radar systems within the limited spectral resources. Traditional orthogonal access methods such as time

division multiple access (TDMA) and frequency division multiple access (FDMA), which split the spectrum into discrete time slots or frequency bands, are unable to achieve the required levels of efficiency. Hence, there is a growing trend in using the same time-frequency resources for simultaneous sensing and communication, an innovative approach more often referred to as integrated sensing and communication (ISaC) or dual functional radar communication (DFRC) [3], which has been shown to offer promising enhancements in spectrum use.

ISaC represents a significant technological convergence in cooperating radar technology with communication systems into a unified platform. This facilitates data collection, transmission, and processing in radar and communication networks [4]. ISaC can have many advantages, including increased spectrum efficiency, enhanced functionality, and improved reliability, as well as many potential applications such as the IoT, smart cities, industrial automation, and healthcare. The unique advantages and practical benefits of ISaC underscore its critical role in advancing the spectral efficiency and capabilities of modern technologies [5].

Similarly, non-orthogonal multiple access (NOMA) is a potential technology for 6G communication networks [6]. This approach is distinct from traditional approaches in that it uses the principle of superposition to multiplex users at the same time and frequency resource, hence improving spectral utilization and efficiency. In doing so, NOMA can significantly increase the system capacity without requiring additional spectral resources. Such advantage of NOMA makes it a key technology for the future 6G networks, which is expected to meet the growing demand for a rapid increase in mobile devices and increased data rate requirements [7].

A. Related work

Many of the existing studies on NOMA systems focus on the bit error rate (BER) performance [8]–[11]. For example, in [8], the authors evaluate the BER performance of a NOMA system with two users having equal distances from the base station under various channel conditions including additive white Gaussian noise (AWGN) and fading environments such as Rayleigh, Rician, Nakagami- m and Weibull. On the other hand, the authors in [9] investigated the performance of the symbol error rate (SER) and the BER in NOMA systems considering the direction of transmission, the number of information streams, and the effects of channel coding. Furthermore, a joint Gray coding scheme was proposed to significantly

Haofeng Liu and Emad Alsusa are with the Department of Electrical and Electronic Engineering, The University of Manchester, Manchester, M13 9PL, United Kingdom. (email: haofeng.liu@postgrad.manchester.ac.uk, e.alsusa@manchester.ac.uk).

Arafat Al-Dweik is with 6G Reserch Center, Department of Computer and Communications Engineering, Khalifa University, Abu Dhabi, 127788, United Arab Emirates (e-mail: arafat.dweik@ku.ac.ae, dweik@fulbrightmail.org)

reduce SER and BER in downlink transmissions. In [10], the authors focused on enhancing NOMA, and presented exact and asymptotic BER expressions under Rayleigh fading conditions for NOMA systems with varying user counts, receiving antennas, and modulation types, including binary phase shift keying (BPSK) and quadrature amplitude modulation (QAM). Additionally, the study derived bounds for the power coefficients to ensure fairness and address constellation ambiguity for systems with two and three users across different modulation orders. The findings highlighted that the range of feasible power coefficients narrows as either the number of users or the modulation complexity increases, exacerbating inter-user interference and impacting BER. The authors in [11] addressed the gaps in NOMA BER analysis by considering the transformation of the noise probability density function (PDF) after using successive interference cancellation (SIC). The first derivation of the exact noise PDF post-SIC as a truncated Gaussian mixture was presented, and highlighted the need for different models for successful and unsuccessful SIC scenarios which significantly improved the accuracy of BER calculation in NOMA systems.

The combination of NOMA and ISaC has also been studied in [12]–[15]. The authors in [12] introduced a NOMA-assisted orthogonal time–frequency space (OTFS) network for ISaC, utilizing UAV as air base station (BS). The system leveraged ISaC to gather positional and velocity data from the user’s echo signals, enhancing system performance through non-orthogonal power allocation tailored for optimal achievable sum rate (ASR). Furthermore, the paper developed a robust power allocation strategy that addresses max-min fairness and maximum ASR issues under both perfect and imperfect channel state information (CSI). The simulation results affirmed the superiority of the proposed NOMA-assisted OTFS-ISaC system in achieving higher rates compared to other systems. A novel semi-ISaC framework was proposed in [13] that offered a flexible bandwidth allocation between exclusive wireless communication, radar detection and integrated ISaC transmission. The paper compared the bandwidth efficiency of semi-ISaC networks that transition from orthogonal multiple access (OMA) to NOMA by assessing the probability of outage, the ergodic communication rates, and the ergodic radar estimation information rate. Simulation results showed that NOMA-based Semi-ISaC provides distinct diversity orders for near and far users. In [14], the authors studied a NOMA-based ISaC system in which the base station simultaneously transmits superimposed communication and sensing signals. They proposed an interference cancellation scheme that optimizes these signals to achieve the desired sensing pattern while meeting the SIC and communication user rate requirements. The simulation results showed that the proposed system outperforms the conventional ISaC. In paper [15], the integration of NOMA with IoT networks was explored to enhance global coverage and resource efficiency in satellite communications. The study introduced a dual approach to secure precoding in a low earth orbit satellite system, addressing both perfect and imperfect CSI of potential eavesdroppers. For each scenario, a joint precoding optimization problem was formulated to maximize the sum secrecy rate using strategies such as artificial jam-

ming. The simulation results demonstrated that the proposed NOMA-ISaC scheme outperforms traditional TDMA in terms of sum secrecy rate, while still maintaining effective sensing capabilities.

On the uplink, several NOMA-based ISaC systems were studied [16]–[18]. The authors in [16] derived novel expressions for the probability of communication and sensing rates. The simulation results showed that the ISaC systems outperform traditional frequency division sensing and communications in sensing rates without compromising the communication quality. The simulation results highlighted the effectiveness of NOMA in ISaC performance enhancement. In [17], the authors provided exact and asymptotic analyzes of the outage probabilities for uplink user equipment (UE) and derived the probability of successful detection for the sensing performance. The results indicated that ISaC NOMA outperforms traditional ISaC systems in both communication reliability and sensing accuracy. The work in [18] focused on the uplink signal and communication performance of NOMA-based ISaC systems, particularly examining the impact of SIC ordering on system performance. By deriving the diversity orders, high signal to noise ratio (SNR) slopes, and high-SNR power offsets, the simulation results showed that the SIC order significantly affects the system’s spectral efficiency and communication reliability through modifications in high-SNR power offsets and array gains.

Several studies have shown that rotating the constellation diagrams or applying different phase shifts for different UEs are promising methods to improve the performance of the NOMA systems [19]–[23]. In [19], the authors derived semi-analytical expressions of SER and BER for the joint maximum likelihood (JML) detection of two quadrature phase shift keying (QPSK) signals with varying phase offsets between the users. The closed-form union bound expressions for the user SER and BER across any phase offset and power ratio are also presented, highlighting the unique error rate dynamics that the detection of JML exhibits per user. In [20] a NOMA downlink system is considered over block fading channels. The authors proposed new schemes that employ n -dimensional constellations from the same algebraic lattices in a number field, allowing each user to achieve a full diversity gain without the need for SIC. The paper analyzes and derives upper bounds for the minimum product distances within these schemes under any power allocation factor. The simulation results showed an improved SER compared to traditional NOMA approaches. In [21], the research focused on the NOMA uplink that uses constellation-rotated spacetime line code (CR-STLC) to communicate with a dual antenna access point. The paper presented a mathematical analysis of the BER performance and spatial diversity order in a two-user uplink CR-STLC NOMA setting. Furthermore, the study compared the dynamic and fixed rotation angle optimization techniques, showing that fixed rotation performs similarly to dynamic rotation in practical SNR scenarios with lower computational cost. The authors in [22] presented a novel investigation of optimal inter-constellation rotation for the uplink NOMA, focusing on improving signal distinctiveness using the minimum distance (MD) criterion. This study derived closed-form expressions

for the MD-maximizing rotation angle and its consequently largest MD between joint constellation points across the common modulation schemes. In [23], the authors introduced a novel approach to improve the uplink performance of NOMA by implementing constellation rotation, particularly by improving the efficiency of SIC receivers. An optimal closed-form solution is achieved to maximize the entropy through variational approximation. Theoretical analysis and simulation results reveal that this scheme surpasses traditional NOMA in capacity and bit error rate, especially when the receiver has fewer antennas or when there is a minimal channel gain difference between the users.

B. Motivation and Contribution

From the surveyed literature, the theoretical analysis of BER and the probability of outage has been carried out in a wide range of scenarios. However, the aforementioned papers all considered detection on a symbol by symbol basis. On the contrary, we proposed a novel signaling approach in which the receiver detects the signals over two periods of symbols [24] to enhance the effectiveness of canceling mutual interference between the radar and the communication system. This is achieved by designing the radar waveform to be orthogonal to the communication signals over two symbol periods to make it possible to eliminate interference between the two subsystems. We have showed that the proposed ISaC system offers superior performance for both communication and radar systems. Nevertheless, the results provided in our previous work were simulation based only. Therefore, in this study, our aim is to present an analytical framework of our proposed ISaC system to provide deeper insights into this system. Specifically, we demonstrate an example of the decision bounds and regions, then derive semi-analytical expressions for the BER of the UEs with a fixed phase shift in alternate symbol periods. In addition, closed-form expressions for the BER upper bound and the outage probability are presented. The detailed contributions can be summarized as follows:

- 1) We present a mathematical framework for our ISaC signaling approach and explain the principle of pair-wise symbol detection.
- 2) We demonstrate the decision regions with fixed rotated phase shifts and derive semi-analytical BER expressions for the zero-forcing (ZF) receiver.
- 3) We derive close-form upper bound BER expressions for the JML and ZF receivers with fixed rotated phase shift.
- 4) We derive closed-form expressions for the capacity outage probability of the JML and ZF receivers, respectively, and average the JML receiver over the Gamma distribution and over the inverse-Gamma distribution for the ZF receiver.
- 5) We present comprehensive results and discussion of the ISaC system under consideration and discuss various performance trade-offs.

Notation: In this paper, the following notation is used. Lowercase bold letters denote vectors (e.g., \mathbf{h}), and uppercase bold letters denote matrix (e.g., \mathbf{H}). For a vector \mathbf{a} , \mathbf{a}^\dagger , \mathbf{a}^* , \mathbf{a}^H , and $\|\mathbf{a}\|$ represent the transpose, conjugate, Hermitian

TABLE I
LIST OF ABBREVIATIONS

Abbreviation	Description
6G	6th generation
ASR	achievable sum rate
AWGN	additive white Gaussian noise
BER	bit error rate
BPSK	binary phase shift keying
BS	base station
CR-STLC	constellation-rotated spacetime line code
CSI	channel state information
DFRC	dual functional radar communication
FDMA	frequency division multiple access
IoT	Internet of Things
ISaC	integrated sensing and communication
JML	joint maximum likelihood
LSB	least significant bit
MD	minimum distance
ML	maximum likelihood
MSB	most significant bit
NOMA	non-orthogonal multiple access
OMA	orthogonal multiple access
OTFS	orthogonal time–frequency space
PDF	probability density function
QAM	quadrature amplitude modulation
QPSK	quadrature phase shift keying
RCS	radar cross section
SER	symbol error rate
SIC	successive interference cancellation
SINR	signal to interference plus noise ratio
SNR	signal to noise ratio
TDMA	time division multiple access
UAV	unmanned aerial vehicle
UE	user equipment
ZF	zero-forcing

transpose, and l_2 norm of \mathbf{a} , respectively. For a scalar B , $|B|$ represents the l_2 norm of B . Furthermore, the expectation value is denoted as $\mathbb{E}[\cdot]$, and the determinant value is denoted as $\det(\cdot)$. Finally, $\mathcal{CN}(\mu, \Omega)$ denotes the complex Gaussian distribution with mean μ and variance Ω .

C. Paper Organization

The rest of the paper is organized as follows. In Sec.II, the communication and radar channel models are given and the proposed signaling architecture is reviewed. In Sec.III, the decision bounds and regions are presented with a given example; then the derivation of the semi-analytical BER expression is given. In Sec.IV, we derive closed-form expressions for the upper bound of the BER of both ZF and JML receiver. Furthermore, in Sec.V, we consider the reliability of the communication system by analyzing the probability of system outage. Finally, the simulation results and discussion are presented in Sec.VI, and Sec.VII concludes the paper. The glossary of this paper is provided in the Table I.

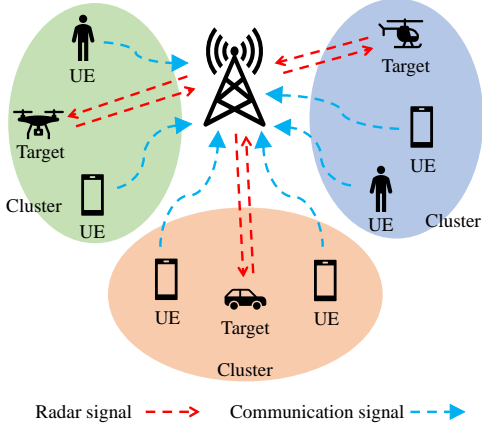


Fig. 1. System model.

II. SYSTEM MODEL

This work considers a system in which a NOMA-based BS simultaneously operates uplink data communication and radar sensing. For simplicity and without loss of generality, we assume that each cluster accommodates $K = 2$ UEs and a single radar target, as presented in Fig. 1. In addition, each UE is equipped with a single antenna. The BS is designed with two distinct sets of antennas, one set is dedicated to communication and the other for radar operations. Furthermore, the BS has M antennas to receive both communication and radar echoes.

A. Communication Channel Model

In this study, the communication channel between the k th UE and the m th BS antenna is denoted as $h_{m,k} = \hat{h}_{m,k}\beta_k$, where $\hat{h}_{m,k} \sim \mathcal{CN}(0,1)$ is the small-scale fading and β_k is the large-scale fading factor of the k th UE, which is given by $\beta_k = d_k^{-\alpha}$, where d_k represents the distance between the k th UE and BS, and α represents the path loss exponent of the communication channel. Consequently,

$$\mathbf{h}_k = [h_{1,k}, h_{2,k}, \dots, h_{M,k}]^\dagger \in \mathbb{C}^{M \times 1}. \quad (1)$$

We assume that BS has perfect knowledge of the CSI, the communication channel is time-invariant between channel estimates, and UE₁ is closer to BS, that is, $d_1 < d_2$ and $\mathbb{E}[\|\mathbf{h}_1\|^2] \geq \mathbb{E}[\|\mathbf{h}_2\|^2]$.

B. Radar Channel Model

For the case where one target is assigned for each resource block, the gain of the two-way radar channel can be calculated based on [25, Eq. 2.8],

$$\dot{g} = \frac{\lambda}{8R^2} \sqrt{\frac{G_t G_r \sigma}{\pi^3}} \quad (2)$$

where G_t and G_r represent the gains of transmit and receive antennas, respectively, σ is the radar cross section (RCS) of the target, R is the distance from the target to the BS, and λ is the signal wavelength. Using the general expression of the

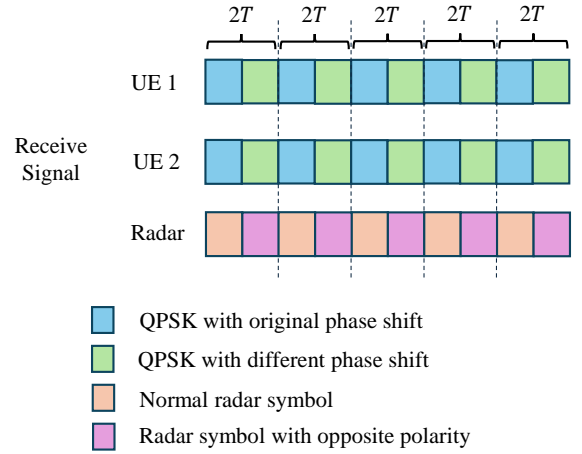


Fig. 2. The proposed signalling model of the ISaC system.

radar channel given in [26, Eq. 1], the radar channel between the target and the m th BS antenna can be represented as

$$g_m = \dot{g} e^{-j2\pi\Theta} e^{j2\pi f_d \mu T} \quad (3)$$

where $e^{-j2\pi\Theta}$ is the phase shift component, which consists of the distance information of the target, $\Theta = 2R/c_0$, where c_0 is the speed of light. The second phase shift term $e^{j2\pi f_d \mu T}$ contains the velocity information of the target, f_d is the Doppler shift, $f_d = 2v f_c / c_0$, where v is the velocity of the target, and f_c is the signal carrier frequency. Furthermore, T is the duration of the symbol, and μ is the symbol index. Therefore, the radar channel vector is given by

$$\mathbf{g} = [g_1, g_2, \dots, g_M]^\dagger \in \mathbb{C}^{M \times 1}. \quad (4)$$

C. The Signaling Model Under Consideration

Conventional NOMA detectors operate under the strict constraint that the power difference between the signals received from different users must exceed a specific threshold [27]. However, in practical scenarios, such a condition is not always feasible, given the fluctuating nature of the signal power received. To address this challenge, a novel ISaC signaling model is proposed in [24], with the assumption that the radar and UE channels remain constant for the duration of two consecutive radar symbols [28]. As shown in Fig. 2, to ensure auto-cancellation of the radar signal at the receiving end, the radar transmitter emits each symbol twice, but alternating its polarity in the second symbol period, e.g. s_r in the first period and $-s_r$ in the second. Therefore, the signal received at the m th BS antenna over two T can be defined as [29],

$$y_m = \begin{cases} \sum_{k=1}^2 \sqrt{P_k} h_{m,k} x_{k,1} + \sqrt{P_r} g_m s_r + n_{m,1}, & t \in T_1 \\ \sum_{k=1}^2 \sqrt{P_k} h_{m,k} x_{k,2} - \sqrt{P_r} g_m s_r + n_{m,2}, & t \in T_2 \end{cases} \quad (5)$$

where $n_{m,t}$ represents the noise in the t th period of the m th receive antenna, which follows the Gaussian distribution with zero mean and σ_n^2 variance. Furthermore, P_k denotes the transmit power of the k th UE, the total communication

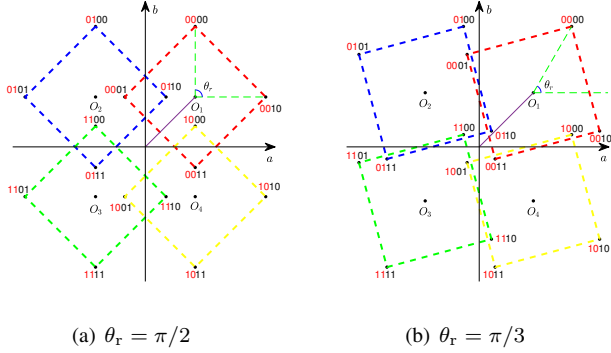


Fig. 3. The constellation diagram of symbols combined $2T$ with different θ_r .

power is $P_{\text{com}} = P_1 + P_2$, and P_r denotes the transmit power of the radar signal. In addition, $x_{k,t}$ denotes the transmitted communication symbol of the k th UE at the t th period. By adding the received signals of both periods, we can obtain

$$y_m = \sqrt{P_1}h_{m,1}x'_1 + \sqrt{P_2}h_{m,2}x'_2 + n'_m, \quad (6)$$

where $x'_1 = x_{1,1} + x_{1,2}$, $x'_2 = x_{2,1} + x_{2,2}$ and $n'_m = n_{m,1} + n_{m,2}$. Therefore, the radar signal is canceled regardless of its power level, and the remaining signals are pure communication signals over two symbol periods. After combining the signals of all M antennas, the signal received over $2T$ is given by

$$\begin{aligned} \mathbf{y}_{2T} &= \begin{bmatrix} h_{1,1} & h_{2,1} & \cdots & h_{M,1} \\ h_{1,2} & h_{2,2} & \cdots & h_{M,2} \end{bmatrix}^\dagger \begin{bmatrix} \sqrt{P_1}x'_1 \\ \sqrt{P_2}x'_2 \end{bmatrix} + \begin{bmatrix} n'_1 \\ \vdots \\ n'_M \end{bmatrix} \\ &= \sqrt{P_k} \mathbf{H} \mathbf{x} + \mathbf{n}. \end{aligned} \quad (7)$$

It should be noted that, since we combine symbols over two T for both UEs, a detection ambiguity will occur if two symbols are of opposite polarity, such as $x_{1,1} = -x_{1,2}$, resulting in cancelation of the communication signal at the receiver. To resolve the ambiguity problem, we propose using alternate phase shifts on adjacent communication symbols. Fig. 3 illustrates the different phase shifts with QPSK modulation as an example, where θ_o represents the original phase shift angle, and θ_r represents the rotated phase shift angle. Specifically, the communication symbols in T_1 are selected from the original phase shift modulation, and the communication symbols in T_2 are selected from a constellation with the different phase shifts. By setting θ_r to a fixed value, the UEs' data are guaranteed to remain non-zero over two T periods. For this to work, the BS must have prior knowledge of the transmission protocol.

Compared to conventional NOMA, the proposed ISaC system does not require much increase in complexity, as it only requires three additional operations, which are to: sum over two T , invert the radar symbol every other T , and multiply each transmitted symbol by $e^{j(\theta_r - \theta_o)}$ every other T .

III. BER ANALYSIS OF THE ZF RECEIVER

As the decoding order in the ISaC systems is difficult to determine, SIC receivers may not be applicable. On the one hand, if the system first decodes the communication signal,

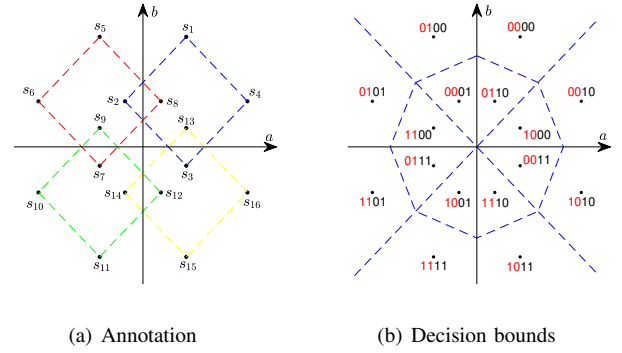


Fig. 4. A possible symbol annotation and decision bounds

the communication ASR will be limited by interference from the sensing signal. On the other hand, it is not always possible to first decode and remove the radar signal, since the power of the received radar signal may be lower than that of the communication signal due to the two-way transmission [30].

By introducing a new matrix $\mathbf{H} = [\mathbf{h}_1, \mathbf{h}_2]$, the ZF receiver is denoted by $\mathbf{W}_{\text{ZF}} \in \mathbb{C}^{2 \times M}$, which is given by

$$\mathbf{W}_{\text{ZF}} = (\mathbf{H}^H \mathbf{H})^{-1} \mathbf{H}^H, \quad (8)$$

or the pseudo-inverse of the channel matrix \mathbf{H} . The signal after the ZF receiver is given by

$$\begin{aligned} \hat{\mathbf{y}}_{\text{ZF}} &= \mathbf{W}_{\text{ZF}} \mathbf{y}_{2T} = \mathbf{W}_{\text{ZF}} \sum_{k=1}^K \sqrt{P_k} \mathbf{h}_k x'_k + \mathbf{W}_{\text{ZF}} \mathbf{n}_{2T} \\ &= \begin{bmatrix} \sqrt{P_1} x'_1 + \mathbf{w}_1 \mathbf{n}_{2T} \\ \sqrt{P_2} x'_2 + \mathbf{w}_2 \mathbf{n}_{2T} \end{bmatrix}, \end{aligned} \quad (9)$$

since $\|\mathbf{w}_k \mathbf{h}_k\|^2 = 1$ and $\|\mathbf{w}_k \mathbf{h}_j\|^2 = 0$. After the ZF receiver, the maximum likelihood (ML) can be used to decode the signal of each UE. By dividing the received signals to the power of each UE, the signal sent to the ML processor is given by

$$\hat{\mathbf{y}} = \begin{bmatrix} x'_1 + \mathbf{w}_1 \mathbf{n}_{2T} / \sqrt{P_1} \\ x'_2 + \mathbf{w}_2 \mathbf{n}_{2T} / \sqrt{P_2} \end{bmatrix}, \quad (10)$$

where the only disturbance encountered during each UE's detection process is due to noise. The power of noise of each UE is given by

$$P_N^{(1)} = \frac{2\sigma_n^2 [(\mathbf{H}^H \mathbf{H})^{-1}]_{1,1}}{P_1}, \quad (11)$$

$$P_N^{(2)} = \frac{2\sigma_n^2 [(\mathbf{H}^H \mathbf{H})^{-1}]_{2,2}}{P_2}, \quad (12)$$

where $\mathbb{E}[\|\mathbf{n}_{2T}\|^2] = 2\sigma_n^2$ because the noise power is computed over $2T$.

To simplify the discussion, the possible annotation for the symbols combined over $2T$ of each UE are given in Fig. 4(a). Let vector \mathbf{s} denotes all 16 possible combined symbols, a_n and b_n are the x coordinate and y coordinate

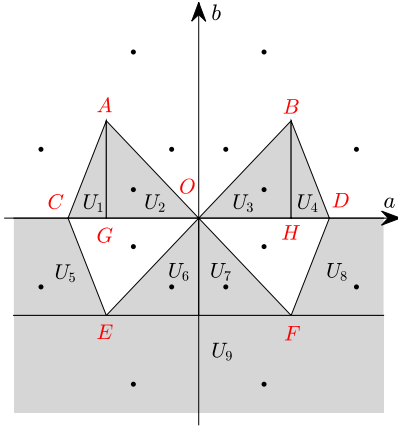


Fig. 5. The error decision regions.

of n th combined symbol, respectively. Therefore, for $n = 1, 2, \dots, 16$, $\mathbf{s}_n = a_n + b_n i$, a_n and b_n are given by

$$a_n = \cos\left(\left\lceil \frac{n}{4} \right\rceil \frac{\pi}{2} - \frac{\pi}{4}\right) + \cos\left[\frac{(2n-1)\pi}{4} + \theta_r\right], \quad (13)$$

$$b_n = \sin\left(\left\lceil \frac{n}{4} \right\rceil \frac{\pi}{2} - \frac{\pi}{4}\right) + \sin\left[\frac{(2n-1)\pi}{4} + \theta_r\right], \quad (14)$$

where $\lceil \cdot \rceil$ denotes the ceiling operation. Recall (10), by sending each element of $\hat{\mathbf{y}}$ to the ML receiver, the symbols can be decoded by applying the decision bounds shown in Fig. 4(b). Hence, the ML receiver for the k th UE is given by

$$\begin{aligned} \{\hat{x}_{k,1}, \hat{x}_{k,2}\} &= \arg \min_{x_{k,1}, x_{k,2} \in \mathcal{S}} |\hat{y}_k - x_{k,1} - x_{k,2}|^2 \\ &= \arg \min_{s_n \in \mathcal{S}} |\hat{y}_k - s_n|^2. \end{aligned} \quad (15)$$

Furthermore, the PDF of $\hat{\mathbf{y}}_k$ given information $x_{k,1}, x_{k,2}$ is

$$f(\hat{y}_k | x_{k,1}, x_{k,2}) = \frac{1}{\pi P_N^{(k)}} e^{-\frac{|\hat{y}_k - x_{k,1} - x_{k,2}|^2}{P_N^{(k)}}}. \quad (16)$$

We now focusing on the BER analysis. For instance, consider the symbol s_8 with the combined bit sequence ‘0110’. In this case, the desired most significant bit (MSB) is ‘0’, and an error detection event would occur if the MSB is mistakenly detected as ‘1’. The regions associated with this error detection correspond to areas U_1 to U_9 , as shown in Fig. 5.

It is clear that the correct transmitted joint symbol set is $E_c = [s_1, s_2, \dots, s_8]$, and the error decoded symbol set is $E_e = [s_9, s_{10}, \dots, s_{16}]$. Let $P(E_c | s_n)$ be the probability that the MSB of the symbol is ‘0,’ thus $P(E_c | s_n) = 1/8$. Recall (13), (14) and (16), the PDF of error detection is given by

$$f(\hat{y}_k | s_n) = \frac{1}{\pi P_N^{(1)}} e^{-\frac{|\hat{y}_k - s_n|^2}{P_N^{(1)}}} = f_{n(a)}(a - a_n) f_{n(b)}(b - b_n). \quad (17)$$

where $f_{n(a)}(a - a_n) = \frac{1}{\sqrt{\pi P_N^{(1)}}} e^{-a^2/P_N^{(1)}}$ and $f_{n(b)}(b - b_n) = \frac{1}{\sqrt{\pi P_N^{(1)}}} e^{-b^2/P_N^{(1)}}$ due to the isotropic symmetry of white Gaussian noise. Therefore, BER for the k th UE is given by

$$\begin{aligned} P_{b,k} &= \sum_{n=1}^8 \int_U P(E_c | s_n) f(\hat{y}_k | s_n) d\hat{\mathbf{y}}_k \\ &= \frac{1}{8} \sum_{n=1}^8 \int \int_U f_{n(a)}(a - a_n) f_{n(b)}(b - b_n) dadb. \end{aligned} \quad (18)$$

Furthermore, the regions U_1, U_2, \dots, U_9 are given by

$$U_1 : \{(a, b) \mid a_C \leq a \leq a_A, b_C \leq b \leq k_{AC}(a - a_C)\} \quad (19a)$$

$$U_2 : \{(a, b) \mid a_G \leq a \leq a_O, b_O \leq b \leq k_{OA}(a - a_O)\} \quad (19b)$$

$$U_3 : \{(a, b) \mid a_O \leq a \leq a_H, b_O \leq b \leq k_{OB}(a - a_O)\} \quad (19c)$$

$$U_4 : \{(a, b) \mid a_H \leq a \leq a_D, b_D \leq b \leq k_{BD}(a - a_D)\} \quad (19d)$$

$$U_5 : \{(a, b) \mid a \leq (b - b_E)/k_{CE} + a_E, b_E \leq b \leq b_C\} \quad (19e)$$

$$U_6 : \{(a, b) \mid a_E \leq a \leq a_O, b_E \leq b \leq k_{OE}(a - a_O)\} \quad (19f)$$

$$U_7 : \{(a, b) \mid a_O \leq a \leq a_F, b_F \leq b \leq k_{OF}(a - a_O)\} \quad (19g)$$

$$U_8 : \{(a, b) \mid (b - b_F)/k_{DF} + a_F \leq a, b_F \leq b \leq b_D\} \quad (19h)$$

$$U_9 : \{(a, b) \mid b \leq b_F\}, \quad (19i)$$

where a_A means the coordinate of A on x-axis, b_A means the coordinate of A on y-axis, k_{AC} means the slope of line AC . Due to the symmetry of the error regions and constellation diagram of \mathbf{s}_n , it is easy to get $(a_B, b_B) = (-a_A, b_A) = (a_F, -b_F) = (-a_E, -b_E)$, $a_B = a_H = -a_G$, $a_D = -a_C$, $k_{AC} = k_{DF} = -k_{BD} = -k_{CE}$, and $k_{OB} = k_{OE} = -k_{OA} = -k_{OF} = 1$. By using the Q function $Q(x) = \frac{1}{\sqrt{2\pi}} \int_x^\infty \exp\left(-\frac{u^2}{2}\right) du$, then substituting (19) into (18) and simplifying them, the BER for UE₁ is given in (20)

where $\rho_k = \sqrt{P_N^{(k)}}/2$.

The BER expression is based on the random variable $\chi_k = \left[(\mathbf{H}^H \mathbf{H})^{-1} \right]_{k,k}$. The χ_k follows the inverse-Gamma distribution [31], which PDF is given by

$$f(\chi_k; \alpha_{ZF}, \beta_{ZF,k}) = \frac{\beta_{ZF,k}^{\alpha_{ZF}}}{\Gamma(\alpha_{ZF})} (1/\chi_k)^{\alpha_{ZF}+1} \exp(-\beta_{ZF,k}/\chi_k), \quad (21)$$

where $\alpha_{ZF} = M - K + 1$, $\beta_{ZF,k} = 1/\beta_k$, and $\Gamma(\cdot)$ means the Gamma function. Therefore, after averaging over the inverse Gamma distribution, the semi-analytical BER for the k th UE is given by

$$P'_{b,k} = \int_0^\infty P_{b,k} f(\chi_k; \alpha_{ZF}, \beta_{ZF,k}) d\chi_k. \quad (22)$$

IV. CLOSED-FROM UPPER BOUND BER EXPRESSION

A. Properties and rules of the outage probability evaluation

With the fixed phase shift $\theta_r = \pi/2$, we summarize the key properties when considering the outage probability as follows.

- 1) *Symmetry*. For each individual bit, only one case needs to be considered, that is, the correct bit equal to ‘0’ or ‘1’. As shown in Fig. 4, the value for each single bit can only be ‘0’ or ‘1’. Thus, when considering each independent bit, when the correct value is ‘0’, the set

$$\begin{aligned}
P_{b,k} = \frac{1}{8} \sum_{n=1}^8 \left\{ 1 + Q\left(\frac{-b_n}{\rho_k}\right) \left[Q\left(\frac{a_D + a_n}{\rho_k}\right) - Q\left(\frac{a_D - a_n}{\rho_k}\right) \right] + Q\left(\frac{b_B + b_n}{-\rho_k}\right) \left[Q\left(\frac{a_B + a_n}{-\rho_k}\right) - Q\left(\frac{a_B - a_n}{\rho_k}\right) \right] \right\} \\
- \frac{1}{8\sqrt{\pi P_N^{(k)}}} \left\{ \int_{-b_B}^0 \left[Q\left(\frac{b + b_B}{-\rho_k k_{AC}} - \frac{a_B + a_n}{\rho_k}\right) + Q\left(\frac{b + b_B}{\rho_k k_{AC}} + \frac{a_B - a_n}{\rho_k}\right) \right] e^{-\frac{(b-b_n)^2}{P_N^{(k)}}} db \right. \\
+ \int_{-a_D}^{-a_B} Q\left(\frac{k_{AC}(a + a_D) - b_n}{\rho_k}\right) e^{-\frac{(a-a_n)^2}{P_N^{(k)}}} da + \int_{-a_B}^0 \left[Q\left(\frac{a + b_n}{-\rho_k}\right) + Q\left(\frac{a - b_n}{\rho_k}\right) \right] e^{-\frac{(a-a_n)^2}{P_N^{(k)}}} da \\
\left. + \int_0^{a_B} \left[Q\left(\frac{a - b_n}{\rho_k}\right) + Q\left(\frac{a + b_n}{-\rho_k}\right) \right] e^{-\frac{(a-a_n)^2}{P_N^{(k)}}} da + \int_{a_B}^{a_D} Q\left(\frac{-k_{AC}(a - a_D) - b_n}{\rho_k}\right) e^{-\frac{(a-a_n)^2}{P_N^{(k)}}} da \right\}. \quad (20)
\end{aligned}$$

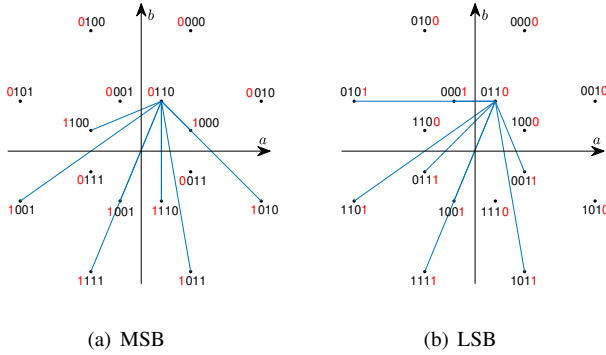


Fig. 6. The set for minimum Euclidean distances when correct value equal to 0. (a) MSB. (b) LSB.

of minimum Euclidean distances between the correct and wrong signals \mathbf{s}_n is exactly the same as when the correct value is '1', since the new constellation diagram is symmetric about the coordinate axis.

- 2) *Identically*. For each bit of any superimposed signal \mathbf{s}_n , the set of minimum Euclidean distances is the same, so only one bit need to be considered. As shown in Fig. 6, the error detection distances for the MSB and least significant bit (LSB) of the bit sequence '0110' are illustrated separately. It is easy to verify that the distance sets for the MSB and the LSB are the same.

Therefore, based on these two properties, for k th UE, only one case for one bit needs to be considered. For simplicity, we consider the situation that the correct value for the MSB of the superimposed signal is '0'.

B. The ZF receiver

As shown in Fig. 4, the symbols with the MSB equal to '0' are $\mathbf{s}_1, \mathbf{s}_2, \dots, \mathbf{s}_8$, and the rest of the symbols $\mathbf{s}_9, \mathbf{s}_{10}, \dots, \mathbf{s}_{16}$ are the symbols with MSB equal to '1'. Let $d_{c,w}^{ZF}$ represent the distance between the symbols \mathbf{s}_c and \mathbf{s}_w . Wrong detection occurs when $n > d_{c,w}^{ZF}/2$, that is,

$$\begin{aligned}
p(n > d_{c,w}^{ZF}/2) \\
= \int_{d_{c,w}^{ZF}/2}^{\infty} \frac{1}{\sqrt{\pi P_N^{(k)}}} \exp\left[\frac{-v^2}{P_N^{(k)}}\right] dv = Q\left(\frac{d_{c,w}^{ZF}}{\sqrt{2P_N^{(k)}}}\right), \quad (23)
\end{aligned}$$

since n follows zero mean and variance $P_N^{(k)}/2$. Furthermore, the distance $d_{c,w}^{ZF}$ when the MSB is equal to '0' is given by

$$d_{c,w}^{ZF} = |\mathbf{s}_c - \mathbf{s}_w|, c \in \{1, 2, \dots, 8\}, w \in \{9, 10, \dots, 16\}. \quad (24)$$

Therefore, the upper bound of BER for the k th UE with the MSB equal to '0' is given by

$$P_{ZF,k}^{\text{upper}}(\text{first bit} = 0) \leq \frac{1}{8} \sum_{c=1}^8 \sum_{w=9}^{16} Q\left(\frac{d_{c,w}^{ZF}}{\sqrt{2P_N^{(k)}}}\right). \quad (25)$$

As we discussed previously, $P_N^{(k)}$ is based on the random variable $\chi_k = [(\mathbf{H}^H \mathbf{H})^{-1}]_{k,k}$, which follows the inverse-Gamma distribution. The unconditional upper bound BER for the k th UE is given in (26), where $A = \sqrt{\frac{P_k (d_{c,w}^{ZF})^2}{4\sigma_n^2}}$, and ${}_2F_1(\cdot)$ is the Hypergeometric function.

C. The JML receiver

The JML receiver tends to decode the signal that has the highest probability which is given by

$$\hat{\mathbf{x}}' = \arg \min_{\mathbf{x}'_1, \mathbf{x}'_2 \in \mathbf{s}} \left\| \mathbf{y}_{2T} - \sqrt{P_1} \mathbf{h}_1 \mathbf{x}'_1 - \sqrt{P_2} \mathbf{h}_2 \mathbf{x}'_2 \right\|^2. \quad (27)$$

Since the JML receiver decodes two UEs' signals simultaneously, there are a total of $16 \times 16 = 256$ possibilities. The position of each possibility is given by $\sqrt{P_1} \|\mathbf{h}_1\| x'_1 + \sqrt{P_2} \|\mathbf{h}_2\| x'_2$. Similarly, assume that the correct MSB for UE₁ is 0, the correct symbols for x'_1 are s_1, s_2, \dots, s_8 , and the wrong detection happens when x'_1 equals $s_9, s_{10}, \dots, s_{16}$, regardless of the symbol x'_2 . Therefore, by letting s_c, s_p to be the correct signals, and s_w, s_q to be the wrong signals for UE₁ and UE₂, respectively, the distances between the correct and wrong symbol positions for JML receiver are given by

$$\begin{aligned}
d_{c,w}^{\text{JML},1} = \left\| \sqrt{P_1} \mathbf{h}_1 (s_c - s_w) + \sqrt{P_2} \mathbf{h}_2 (s_p - s_q) \right\|, \\
c \in \{1, 2, \dots, 8\}, w \in \{9, 10, \dots, 16\}, p, q \in \{1, 2, \dots, 16\}. \quad (28)
\end{aligned}$$

Based on (23) and (28), the upper bound for UE₁ with the JML receiver is given in (29), which is the conditional upper bound for given \mathbf{h}_1 and \mathbf{h}_2 . With the help of the property of the Gaussian random vector, it is easy to get $\sqrt{P_1} \mathbf{h}_1 (s_c - s_w) + \sqrt{P_2} \mathbf{h}_2 (s_p -$

$$P_{ZF,k}^{\text{upper}} = \frac{1}{8} \sum_{c=1}^8 \sum_{w=1}^8 \int_0^\infty Q \left(\frac{d_{c,w}^{\text{ZF}}}{\sqrt{2P_N^{(k)}}} \right) f(\chi_k; \alpha_{\text{ZF}}, \beta_{\text{ZF}}) d\chi_k = \frac{1}{8} \sum_{c=1}^8 \sum_{w=1}^8 \int_0^\infty Q \left(\frac{A}{\sqrt{\chi_k}} \right) \frac{\beta_{\text{ZF}}^{\alpha_{\text{ZF}}}}{\Gamma(\alpha_{\text{ZF}})} \left(\frac{1}{\chi_k} \right)^{\alpha_{\text{ZF}}+1} \exp \left(-\frac{\beta_{\text{ZF}}}{\chi_k} \right) d\chi_k$$

$$= \frac{1}{8} \sum_{c=1}^8 \sum_{w=1}^8 \left[0.5 - \frac{\Gamma(0.5 + \alpha_{\text{ZF}}) {}_2F_1(0.5, 0.5 + \alpha_{\text{ZF}}; 1.5; -A^2 / (2\beta_{\text{ZF}}))}{\sqrt{2\pi\beta_{\text{ZF}}}\Gamma(\alpha_{\text{ZF}})/A} \right] \quad (26)$$

$$P_{\text{JML},1}^{\text{upper}}(\text{first bit} = 0) = \frac{1}{8} \sum_{c=1}^8 \sum_{w=9}^{16} \sum_{p=1}^{16} \sum_{q=1}^{16} Q \left(\frac{\|\sqrt{P_1}\mathbf{h}_1(s_c - s_w) + \sqrt{P_2}\mathbf{h}_2(s_p - s_q)\|}{\sqrt{4\sigma_n^2}} \right) \quad (29)$$

$s_q) \sim \mathcal{CN}(\mathbf{0}, (P_1\beta_1 |s_c - s_w|^2 + P_2\beta_2 |s_p - s_q|^2) \cdot \mathbf{I}_M)$.
Given the new variable,

$$\delta_{c,w,p,q}^1 = \frac{(d_{c,w}^{\text{JML},1})^2}{4\sigma_n^2}, \quad (30)$$

then $\delta_{c,w,p,q}^1$ follows Erlang distribution with mean $M\eta_{c,w,p,q}^1$ and variance $M(\eta_{c,w,p,q}^1)^2$ [32], where $\eta_{c,w,p,q}^1$ is given by

$$\eta_{c,w,p,q}^1 = \frac{P_1\beta_1 |s_c - s_w|^2 + P_2\beta_2 |s_p - s_q|^2}{4\sigma_n^2},$$

$$c \in \{1, 2, \dots, 8\}, w \in \{9, 10, \dots, 16\}, p, q \in \{1, 2, \dots, 16\}. \quad (31)$$

The probability density function of $\delta_{m,n,p,q}^1$ is given by

$$f_{\delta_{c,w,p,q}^1}(\delta) = \frac{\delta^{M-1}}{(M-1)! (\eta_{c,w,p,q}^1)^M} \exp \left(-\frac{\delta}{\eta_{c,w,p,q}^1} \right). \quad (32)$$

Therefore, based on (29)-(32), the unconditional upper bound of BER for UE₁ is given by (33).

Similarly, we assume the first correct bit for UE₂ is 0, the distances between the correct and wrong symbol positions are given by

$$d_{c,w}^{\text{JML},2} = \left\| \sqrt{P_2}\mathbf{h}_2(s_c - s_w) + \sqrt{P_1}\mathbf{h}_1(s_p - s_q) \right\|,$$

$$c \in \{1, 2, \dots, 8\}, w \in \{9, 10, \dots, 16\}, p, q \in \{1, 2, \dots, 16\}. \quad (33)$$

Given a new variable,

$$\delta_{c,w,p,q}^2 = \frac{(d_{c,w}^{\text{JML},2})^2}{4\sigma_n^2}, \quad (34)$$

which follows the Erlang distribution with mean $M\eta_{c,w,p,q}^2$ and variance $M(\eta_{c,w,p,q}^2)^2$ [32], where $\eta_{c,w,p,q}^2$ is given by

$$\eta_{c,w,p,q}^2 = \frac{P_2\beta_2 |s_c - s_w|^2 + P_1\beta_1 |s_p - s_q|^2}{4\sigma_n^2},$$

$$c \in \{1, 2, \dots, 8\}, w \in \{9, 10, \dots, 16\}, p, q \in \{1, 2, \dots, 16\}. \quad (35)$$

Therefore, the unconditional upper bound of the BER for the k th UE with the JML receiver is given in (36).

V. THE OUTAGE PROBABILITY

A. The ZF receiver

The sum rate for k th UE with ZF receiver over $2T$ is given by

$$C_k^{\text{ZF}} = \log_2 \left(1 + \frac{P_k |x'_k|^2}{\left[(\mathbf{H}^H \mathbf{H})^{-1} \right]_{k,k} 2\sigma_n^2} \right). \quad (37)$$

Therefore, the outage probability for k th UE with the ZF receiver is given by

$$P_{\text{ZF},k}^{\text{out}} = 1 - \Pr \left(\log_2 \left(1 + \frac{P_k |x'_k|^2}{\left[(\mathbf{H}^H \mathbf{H})^{-1} \right]_{k,k} 2\sigma_n^2} \right) \geq C \right)$$

$$= 1 - \Pr \left(\left[(\mathbf{H}^H \mathbf{H})^{-1} \right]_{k,k} \leq R_{\text{ZF}} \right), \quad (38)$$

where C is the minimum rate requirement for the k th UE, and R_{ZF} is given by $\frac{P_k |x'_k|^2}{(2^C - 1) 2\sigma_n^2}$. As we discussed previously, $\chi_k = \left[(\mathbf{H}^H \mathbf{H})^{-1} \right]_{k,k}$ follows the inverse-Gamma distribution, after simplification, the unconditional outage probability for the k th UE with the ZF receiver is given by

$$P_{\text{ZF},k}^{\text{out}} = 1 - \int_0^{R_{\text{ZF}}} f(\chi_k; \alpha_{\text{ZF}}, \beta_{\text{ZF},k}) d\chi_k = 1 - Q \left(\alpha_{\text{ZF}}, \frac{\beta_{\text{ZF},k}}{R_{\text{ZF}}} \right), \quad (39)$$

where $Q(\alpha_{\text{ZF}}, \beta_{\text{ZF},k})$ is the regularized gamma function. Therefore, the outage probability of the ZF receiver can be calculated by averaging the sum of the outage probability of all the UEs.

B. The JML receiver

The sum rate for the k th UE with JML receiver over $2T$ is given by [33]

$$C_k^{\text{JML}} = -\log \left[\det \left(\left(1 + \frac{P_k |x'_k|^2}{2\sigma_n^2} \mathbf{h}_k^H \mathbf{h}_k \right)^{-1} \right) \right]. \quad (40)$$

$$P_{\text{JML},k}^{\text{upper}} = \frac{1}{8} \sum_{c=1}^8 \sum_{w=9}^{16} \sum_{p=1}^{16} \sum_{q=1}^{16} \int_0^\infty Q(\sqrt{\delta}) f_{\delta_{c,w,p,q}^k}(\delta) d\delta = \frac{1}{8} \sum_{c=1}^8 \sum_{w=9}^{16} \sum_{p=1}^{16} \sum_{q=1}^{16} \frac{\Gamma(2M)_2F_1\left(M, M+0.5; M+1; -\frac{2}{\eta_{c,w,p,q}^k}\right)}{2^M (\eta_{c,w,p,q}^k)^M \Gamma(M)}. \quad (36)$$

TABLE II
SYSTEM PARAMETERS.

Parameter	Value	Description
α	3.5	Path loss exponent
f_c	5.8 GHz	Carrier frequency
B	10 MHz	Bandwidth
T	10 μ s	Symbol duration
p_{N0}	-174 dBm/Hz	Noise spectral density
M	5	Number of BS antennas
G_t, G_r	2 dB	Radar antenna gain
σ	0 dBm ²	RCS
θ_o	$\pi/4$	Original phase shift
θ_r	$\pi/2$	Rotated phase shift

Therefore, the outage probability for the k th UE with the JML receiver is given by

$$\begin{aligned} P_{\text{JML},k}^{\text{out}} &= \Pr\left(-\log\left[\det\left(\left(1 + \frac{P_k |x'_k|^2}{2\sigma_n^2} \mathbf{h}_k^H \mathbf{h}_k\right)^{-1}\right)\right] \leq C\right) \\ &= \Pr\left(\mathbf{h}_k^H \mathbf{h}_k \leq R_{\text{JML}}\right), \end{aligned} \quad (41)$$

where C is the minimum rate requirement for the k th UE, and R_{JML} is given by $\frac{(2^C - 1)2\sigma_n^2}{P_k |x'_k|^2}$. The random variable $\xi_k = \mathbf{h}_k^H \mathbf{h}_k$ follows the Gamma distribution, and the PDF is given by

$$f(\xi_k; \alpha_{\text{JML}}, \beta_{\text{JML},k}) = \frac{\beta_{\text{JML},k}^{\alpha_{\text{JML}}}}{\Gamma(\alpha_{\text{JML}})} \xi_k^{\alpha_{\text{JML}}-1} \exp(-\beta_{\text{JML},k} \xi_k), \quad (42)$$

where $\alpha_{\text{JML}} = M$ and $\beta_{\text{JML},k} = 1/\beta_k$. After simplification, the unconditional outage probability for the k th UE with the JML receiver is given by

$$\begin{aligned} P_{\text{JML},k}^{\text{out}} &= \int_0^{R_{\text{JML}}} f(\xi_k; \alpha_{\text{JML}}, \beta_{\text{JML},k}) d\xi_k \\ &= \frac{\gamma(\alpha_{\text{JML}}, \beta_{\text{JML},k} R_{\text{JML}})}{\Gamma(\alpha_{\text{JML}})}, \end{aligned} \quad (43)$$

where $\gamma(\cdot)$ represents the lower incomplete gamma function. Similarly, the outage probability of the JML receiver can be calculated by averaging the sum of the UEs' outage probabilities.

VI. NUMERICAL RESULTS

In our simulation, UE₁ is randomly located in a 30 to 80 m communication range, and the distance of UE₂ is set to $d_2 = 1.2d_1$. For the radar system, only one target is assigned to the same resource block which is randomly located between the radar sensing range of 10 and 50m with speed 10m/s. In addition, QPSK modulation is used for both communication and radar systems. All other parameters used during the simulation are shown in Table II.

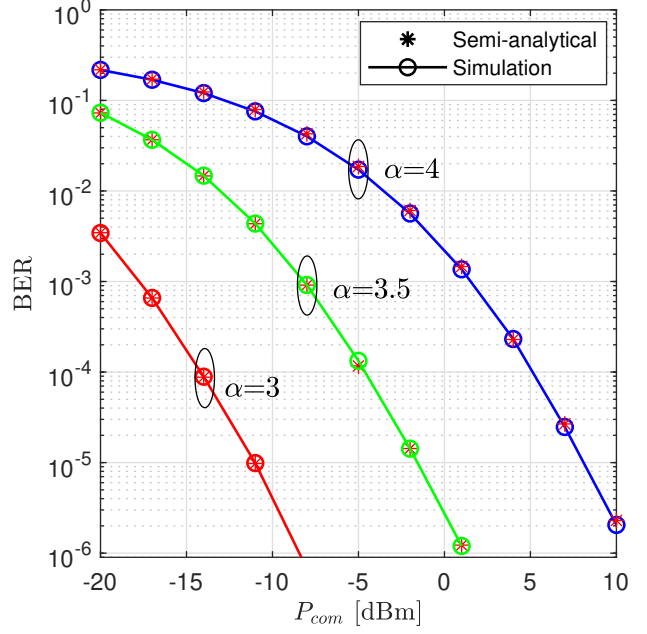


Fig. 7. The semi-analytical theoretical BER performance as a function of UE power P_{com} of ZF receiver and different path loss exponent α .

In Fig. 7, the performance of semi-analytical theoretical BER analysis with the ZF receiver is presented. It is clear that the results of (22) are perfectly matched with the simulation results. Additionally, when considering the different path loss exponents α of the channel, the theoretical results are still aligned with the simulations. Furthermore, increasing the value of α results in a worse channel for the UEs. Since the ZF receiver is used, the noise will be amplified more when the channel is severe. Moreover, the use of the ZF receiver depends greatly on the quality of the channel. When the system has good channel conditions, there is a great performance difference in BER at the same power P_{com} .

Fig. 8 shows the performance difference between the ZF and JML receivers. The BER performances of the JML receiver are consistently better than those of the ZF receiver. When the channel condition is relatively bad and in the lower power P_{com} region, the JML receiver gives a very similar performance compared to the ZF receiver, since even though the JML receiver does not amplify the power of the noise like the ZF receiver, the noise power is relatively high compared to the UEs' power in this situation. When considering a system with good channel conditions, that is, when $\alpha = 3$, it can be found that the JML receiver also performs better than the ZF receiver when the UEs have lower power P_{com} , mainly because the ZF receiver amplifies noise when eliminating inter-

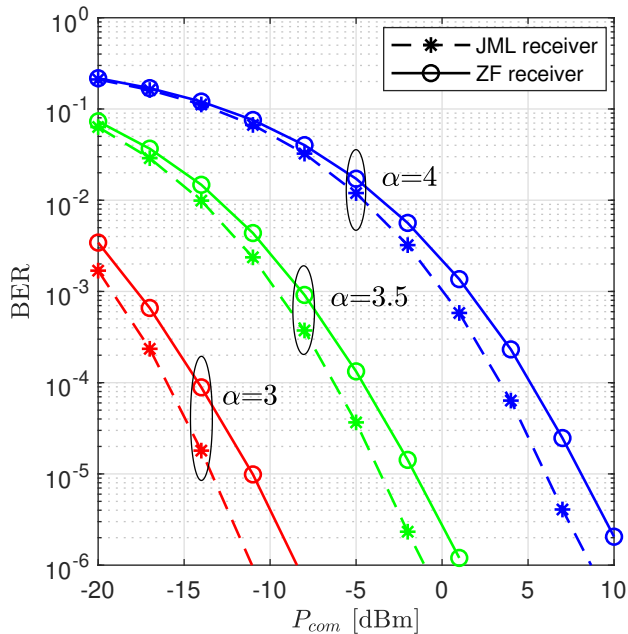


Fig. 8. The performance comparison of BER between ZF and JML receiver as a function of UE power P_{com} with different path loss exponent α .

user interference. Furthermore, the JML receivers generally have significant performance advantages over the ZF receivers, but in the proposed ISaC system, this advantage is not obvious. The main reason is that in the proposed ISaC system, the JML receiver decodes the signals of two UEs simultaneously, that is, it has $16 \times 16 = 256$ constellation points. In addition, since we use different phase shifts on adjacent symbol periods, the minimum Euclidean distance between symbols is not the same. Especially in the range close to the origin point, the distance between adjacent symbols is very small, thus reducing the performance of the JMLs receiver. For the ZFs receiver, it only needs to detect the data of a single UEs separately, so each user only has 16 constellation points, and the minimum Euclidean distance between symbols is also larger than that of the JMLs receiver. So in the proposed ISaCs system, the performance of the JMLs and ZFs receivers is relatively close.

In Fig. 9, the upper bounds of the BER of the ZF receiver with different path loss exponents α are presented. We use the simulation results to demonstrate the exact performance of the BER, and the upper bound of the BER with the ZF receiver is given by (26). When UEs have higher communication power P_{com} , even if channel conditions are worse, for example $\alpha = 4$, the upper bound of BER is almost consistent with the exact BER performance, giving a very close performance. When channel conditions improve, the performance of the upper bound of the BER can be highly similar to that of the real BER even at low power. Therefore, when the channel conditions are acceptable, the system can be evaluated by using the upper bound of BER, thereby reducing the computational complexity and obtaining a very approximate system performance.

In Fig. 10, the upper bounds of the BER of the JML receiver with different path loss exponents α are presented.

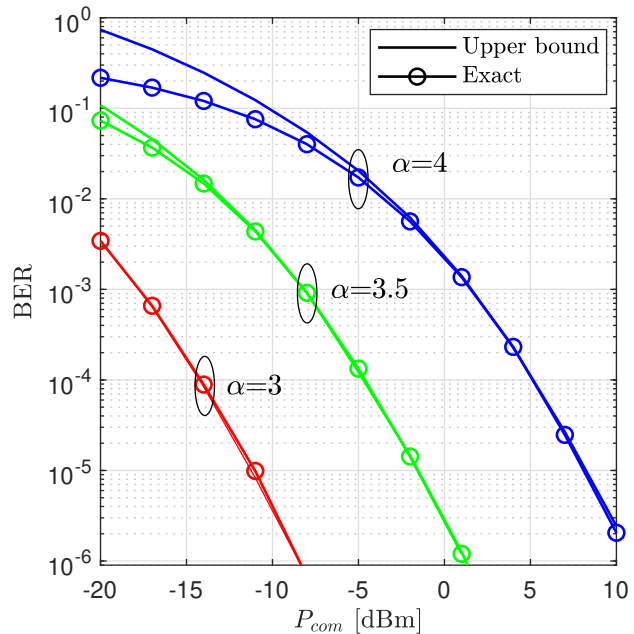


Fig. 9. The performance of BER upper bound of ZF receiver as a function of UE power P_{com} with different path loss exponent α .

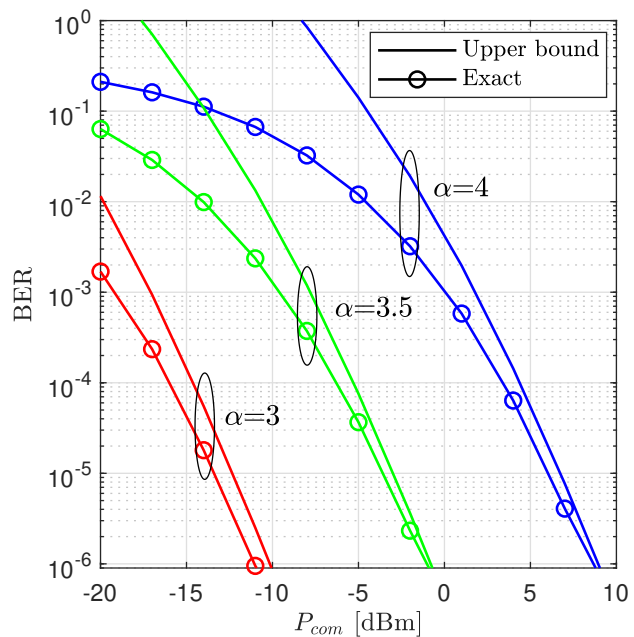


Fig. 10. The performance of BER upper bound of JML receiver as a function of UE power P_{com} with different path loss exponent α .

Similarly, the simulation results are used to show the exact performance of the BER, and the upper bound of the BER with the JML receiver is given by (36). As can be seen in the figure, under a variety of different channel conditions, the upper bound of the BER of the JML receiver does not fit well with the exact performance of BER even in the region with higher communication power. Furthermore, bad channels will cause the difference between the upper bound of the

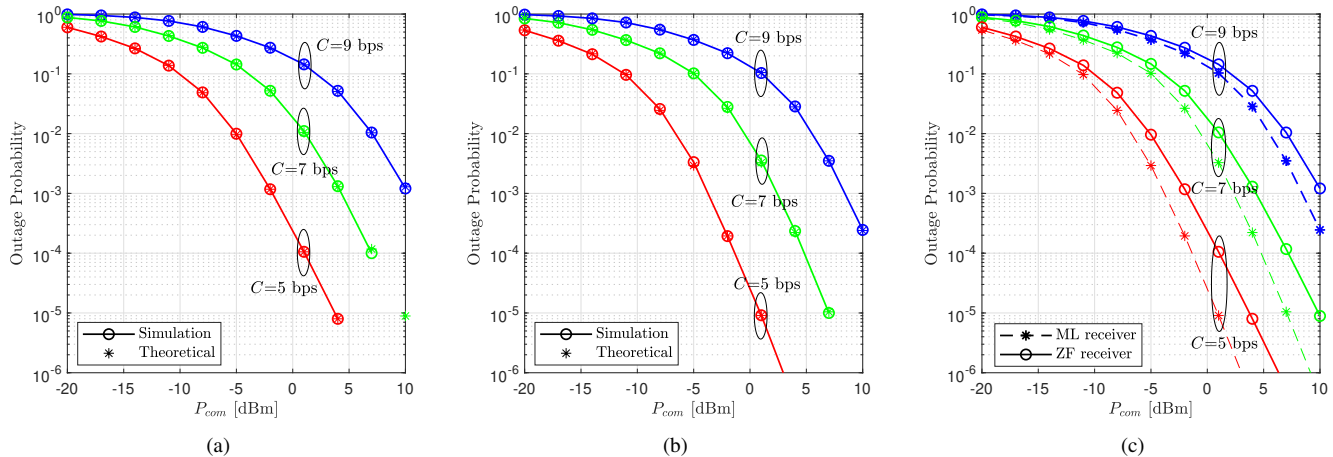


Fig. 11. The performance of outage probability as a function of communication power P_{com} with different minimum ASR requirement C . (a) ZF receiver. (b) JML receiver. (c) Comparison between ZF and JML receiver.

BER and the exact BER to increase significantly in the lower communication power region.

Furthermore, it should be noted that the complexity of calculating the upper bound of the BER of the JML receiver is much greater than that of the ZF receiver. It can be seen from (26) and (36) that since the JML receiver decodes the signals of two UEs in two symbol periods at the same time, the number of $d_{c,w}^{\text{JML},k}$ to be considered is extremely large, while the ZF receiver eliminates the interference between UEs, thus reducing the amount of $d_{c,w}^{\text{ZF}}$ that needs to be considered, resulting in less computational complexity. Furthermore, since there are many possibilities for erroneously decoding signals when using the JML receiver, this results in a large difference between the upper bound of the BER of the JML receiver and the exact BER. When channel conditions worsen, it means a reduction in the SNR at the same power, once again increasing the difference between the upper bound and the exact BER. In contrast, because the ZF receiver only considers the situation of each individual UE, the possibility of error decoding is reduced, and the gap between the upper bound of the BER and the exact value is smaller.

Fig. 11(a) presents the performance of the outage probability with the ZF receiver given the minimum ASR constraints $C = \{5, 7, 9\}$ bps. It shows that the analytical results given by (39) are perfectly matched to the simulation results. Furthermore, it is clear that with an increase in the minimum rate requirement C for the UEs, the probability of the system being out of service increases for the same communication power P_{com} . Similarly, Fig. 11(b) also demonstrates the performance of the outage probability with the JML receiver given minimum ASR constraints $C = \{5, 7, 9\}$ bps. Again, the analytical results given in (43) are in perfect agreement with the simulation results. Furthermore, we compare the performance of outage probability with the ZF and JML receiver in Fig. 11(c). Clearly, the JML receiver has better performance compared to the ZF receiver, and the difference between the ZF and the JML receiver tends to be greater with increasing P_{com} . The reason is that at the same value of P_{com} , the communication

ASR of the JML receiver is also higher than that of the ZF receiver, as in [24]. In addition, the ZF receiver will amplify the noise power when canceling the inter-user interference, leading to a lower signal to interference plus noise ratio (SINR); thus, the ZF receiver has a smaller communication ASR compared to the JML receiver at the same communication power P_{com} , which means a higher outage probability.

It should be noted that the computational complexity of the JML receiver is $\mathcal{O}(Q^{2K})$, where Q is the modulation order. Compared to the ZF receiver which has $\mathcal{O}(K^3)$ computational complexity due to matrix inversion operations, the ZF receiver obviously gives a lower system cost. Therefore, although the JML receiver provides better performance in both BER and outage probability, considering the computational cost and the difference in performance, it is better to choose the ZF receiver rather than the JML receiver, which offers a balanced trade-off between system performance and computational complexity.

VII. CONCLUSIONS

In this study, we explore the BER and outage probability of a novel ISaC of NOMA based uplink IoT system, in which detection is done over two symbol periods. We develop a semi-analytical expression to calculate the exact BER of the ZF receiver, and derive closed-form expressions for the upper BER bounds of both the ZF and the JML receivers. In addition, we derive closed-form expressions for the outage probability of both the ZF and JML receivers. The results indicate a strong alignment between the semi-analytical BER and closed-form outage probability expressions with the simulation results. We also examine the upper bound of the BER under varying path loss exponents. Overall, the numerical results showed that the JML receiver performs better in both the BER and the outage probability, especially in higher SNR regions. However, the JML receiver requires a much higher computational cost compared to the ZF receiver, and the performance of the JML receiver is also degraded due to the use of different phase shifts over $2T$. Therefore, the ZF receiver is a balanced

approach when considering the trade-off between the system performance and complexity.

REFERENCES

- [1] W. Saad, M. Bennis, and M. Chen, "A vision of 6g wireless systems: Applications, trends, technologies, and open research problems," *IEEE Network*, vol. 34, no. 3, pp. 134–142, 2020.
- [2] Z. Wei, H. Qu, Y. Wang, X. Yuan, H. Wu, Y. Du, K. Han, N. Zhang, and Z. Feng, "Integrated sensing and communication signals toward 5g-a and 6g: A survey," *IEEE Internet Things J.*, vol. 10, no. 13, pp. 11 068–11 092, 2023.
- [3] A. R. Chiriyath, B. Paul, and D. W. Bliss, "Radar-communications convergence: Coexistence, cooperation, and co-design," *IEEE Trans. Cogn. Commun. Netw.*, vol. 3, no. 1, pp. 1–12, 2017.
- [4] Z. Wei, F. Liu, C. Masouros, N. Su, and A. P. Petropulu, "Toward multi-functional 6g wireless networks: Integrating sensing, communication, and security," *IEEE Communications Magazine*, vol. 60, no. 4, pp. 65–71, 2022.
- [5] Y. Cui, F. Liu, X. Jing, and J. Mu, "Integrating sensing and communications for ubiquitous iot: Applications, trends, and challenges," *IEEE Network*, vol. 35, no. 5, pp. 158–167, 2021.
- [6] Z. Ding and H. V. Poor, "On the application of bac-noma to 6g ummte," *IEEE Commun. Lett.*, vol. 25, no. 8, pp. 2678–2682, 2021.
- [7] F. Liu, L. Zhou, C. Masouros, A. Li, W. Luo, and A. Petropulu, "Toward dual-functional radar-communication systems: Optimal waveform design," *IEEE Trans. Signal Process.*, vol. 66, no. 16, pp. 4264–4279, 2018.
- [8] M. Ranjeeth, V. Manohar, A. S. Supriya, M. Vinay, and M. Bhargav, "Ber analysis using noma system over various fading channels," in *2021 2nd International Conference on Communication, Computing and Industry 4.0 (C2I4)*, 2021, pp. 1–5.
- [9] W. Han, X. Ma, D. Tang, and N. Zhao, "Study of ser and ber in noma systems," *IEEE Trans. Veh. Technol.*, vol. 70, no. 4, pp. 3325–3340, 2021.
- [10] H. Yahya, E. Alsusa, and A. Al-Dweik, "Exact ber analysis of noma with arbitrary number of users and modulation orders," *IEEE Trans. Commun.*, vol. 69, no. 9, pp. 6330–6344, 2021.
- [11] A. Al-Dweik, A. Bedoui, and Y. Iraqi, "On the ber analysis of noma systems," *IEEE Wireless Commun. Lett.*, vol. 13, no. 3, pp. 786–790, 2024.
- [12] L. Xiang, K. Xu, J. Hu, C. Masouros, and K. Yang, "Robust noma-assisted ofts-isac network design with 3-d motion prediction topology," *IEEE Internet Things J.*, vol. 11, no. 9, pp. 15 909–15 918, 2024.
- [13] C. Zhang, W. Yi, Y. Liu, and L. Hanzo, "Semi-integrated-sensing-and-communication (semi-isac): From oma to noma," *IEEE Trans. Commun.*, vol. 71, no. 4, pp. 1878–1893, 2023.
- [14] Z. Wang, Y. Liu, X. Mu, and Z. Ding, "Noma inspired interference cancellation for integrated sensing and communication," in *ICC 2022 - IEEE International Conference on Communications*, 2022, pp. 3154–3159.
- [15] M. Huang, F. Gong, G. Li, N. Zhang, and Q.-V. Pham, "Secure precoding for satellite noma-aided integrated sensing and communication," *IEEE Internet Things J.*, pp. 1–1, 2024.
- [16] C. Ouyang, Y. Liu, and H. Yang, "On the performance of uplink isac systems," *IEEE Commun. Lett.*, vol. 26, no. 8, pp. 1769–1773, 2022.
- [17] M. Liu, M. Yang, and A. Nallanathan, "On the performance of uplink and downlink integrated sensing and communication systems," in *2022 IEEE Globecom Workshops (GC Wkshps)*, 2022, pp. 1236–1241.
- [18] C. Ouyang, Y. Liu, and H. Yang, "Revealing the impact of sic in noma-isac," *IEEE Wireless Commun. Lett.*, vol. 12, no. 10, pp. 1707–1711, 2023.
- [19] C. Liu and N. C. Beaulieu, "Exact ser and ber analysis on jointly optimal maximum likelihood detection of two qpsk signals with phase offset," *IEEE Trans. Veh. Technol.*, vol. 70, no. 11, pp. 11 695–11 709, 2021.
- [20] M. Qiu, Y.-C. Huang, and J. Yuan, "Downlink non-orthogonal multiple access without sic for block fading channels: An algebraic rotation approach," *IEEE Trans. Wireless Commun.*, vol. 18, no. 8, pp. 3903–3918, 2019.
- [21] K.-H. Lee, J. S. Yeom, J. Jeong, and B. C. Jung, "Performance analysis of uplink noma with constellation-rotated stlc for iot networks," *IEEE Open J. Commun. Soc.*, vol. 3, pp. 705–717, 2022.
- [22] C.-H. Lin, S.-L. Shieh, T.-C. Chi, and P.-N. Chen, "Optimal inter-constellation rotation based on minimum distance criterion for uplink noma," *IEEE Trans. Veh. Technol.*, vol. 68, no. 1, pp. 525–539, 2019.
- [23] N. Ye, A. Wang, X. Li, W. Liu, X. Hou, and H. Yu, "On constellation rotation of noma with sic receiver," *IEEE Commun. Lett.*, vol. 22, no. 3, pp. 514–517, 2018.
- [24] H. Liu and E. Alsusa, "A novel isac approach for uplink noma system," *IEEE Commun. Lett.*, vol. 27, no. 9, pp. 2333–2337, 2023.
- [25] M. Richards, J. Scheer, and W. Holm, *Principles of Modern Radar*, ser. Principles of Modern Radar. SciTech Pub., 2010, no. v. 3.
- [26] Y. L. Sit, B. Nuss, and T. Zwick, "On mutual interference cancellation in a mimo ofdm multiuser radar-communication network," *IEEE Trans. on Veh. Technol.*, vol. 67, no. 4, pp. 3339–3348, 2018.
- [27] Y. Iraqi and A. Al-Dweik, "Power allocation for reliable sic detection of rectangular qam-based noma systems," *IEEE Trans. on Veh. Technol.*, vol. 70, no. 8, pp. 8355–8360, 2021.
- [28] K. Zhang, *Wireless Communications: Principles, Theory and Methodology*. Wiley, 2015.
- [29] A. Al-Dweik, E. Alsusa, O. A. Dobre, and R. Hamila, "Multi-symbol rate noma for improving connectivity in 6g communications networks," *IEEE Communications Magazine*, pp. 1–7, 2023.
- [30] X. Mu, Z. Wang, and Y. Liu, "Noma for integrating sensing and communications towards 6g: A multiple access perspective," *IEEE Wireless Communications*, pp. 1–8, 2023.
- [31] P. Li, D. Paul, R. Narasimhan, and J. Cioffi, "On the distribution of sinr for the mmse mimo receiver and performance analysis," *IEEE Trans. Inf. Theory*, vol. 52, no. 1, pp. 271–286, 2006.
- [32] J. S. Yeom, H. S. Jang, K. S. Ko, and B. C. Jung, "Ber performance of uplink noma with joint maximum-likelihood detector," *IEEE Trans. on Veh. Technol.*, vol. 68, no. 10, pp. 10 295–10 300, 2019.
- [33] L. Zhao, X. Sha, F.-C. Zheng, and X. Wu, "Achievable sum rates of mimo sc-fdma systems with different receivers," in *2015 IEEE Wireless Communications and Networking Conference (WCNC)*, 2015, pp. 153–158.